Science Advances
AAAS

Supplementary Materials for

Orally efficacious lead of the AVG inhibitor series targeting a dynamic interface in the respiratory syncytial virus polymerase

Julien Sourimant *et al.*

Corresponding author: Richard K. Plemper, rplemper@gsu.edu

Sci. Adv. **8**, eabo2236 (2022)
DOI: 10.1126/sciadv.abo2236

The PDF file includes:

Other Supplementary Material for this manuscript includes the following:

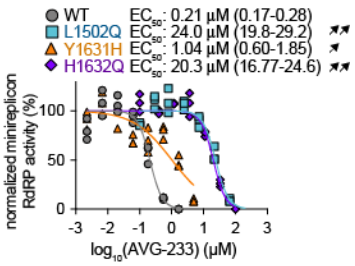

Fig. S1. Dose-response inhibition of RSV minireplicon in presence of resistance mutation candidates. Values are normalized for vehicle-treated reactions; symbols represent individual biological repeats (n=3), determined in nine technical repeats each. EC_{50} values and 95% confidence intervals are derived from 4-parameter variable slope regression models (solid line). Single or double black arrows visualize moderate (EC50 fold change <10) or robust (EC50 fold change >10) resistance, respectively.

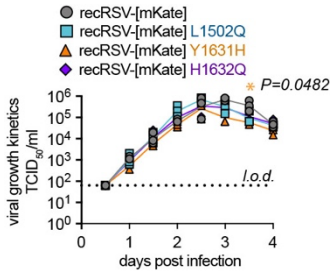

Fig. S2. Multi-step growth curves of recRSV-fireSMASh harboring individual resistance mutations L1502Q, Y1631H, or H1632Q. Symbols represent independent biological repeats and lines connect medians. 2-way ANOVA with Dunnett's post-hoc test.

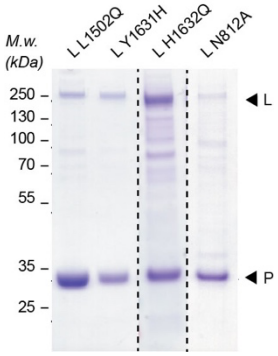

Fig. S3. Purified recombinant RSV RdRP (P-L) with resistance mutations or mutation N812A eliminating polymerase activity (*59*). Coomassie blue staining after SDS-PAGE fractionation; material representing L and P polypeptides is highlighted.

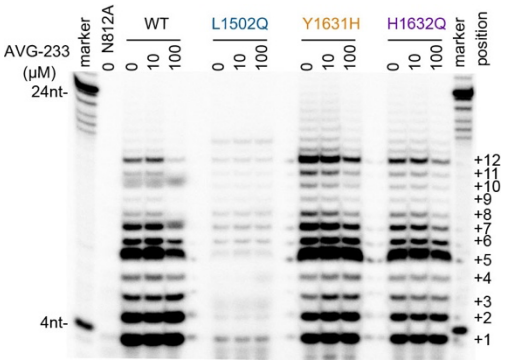

Fig. S4. Representative autoradiogram of primer extension assay from Fig. 1I.

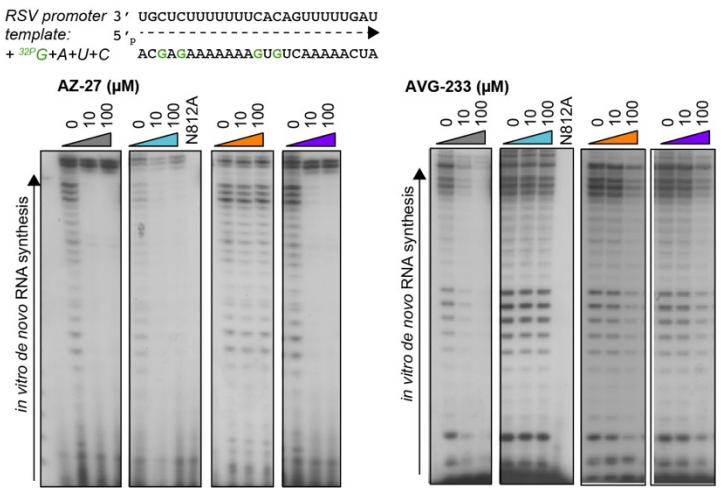

Fig. S5. Side-by side comparison of AVG-233 and AZ-27 in *de novo* RNA synthesis assay using L preparations harboring distinct resistance mutations. Color-coding of L preparations as in Fig. 1D-E.

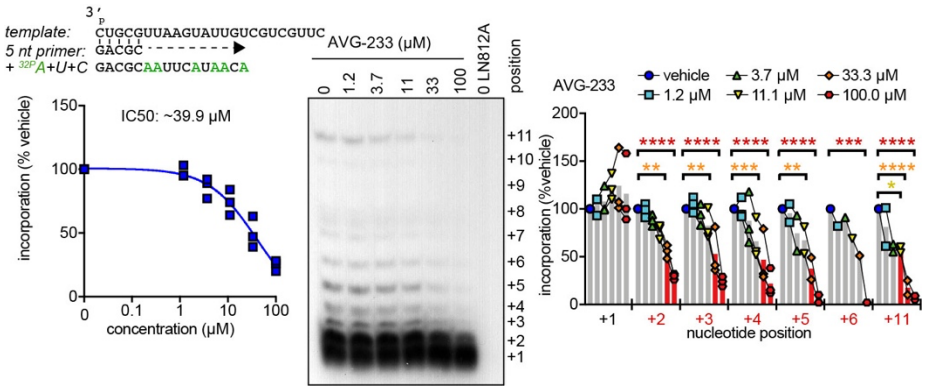

Fig. S6. *In vitro* RdRP assay. The assay was performed as in Fig. 1I, using the alternative primer/template pair shown.

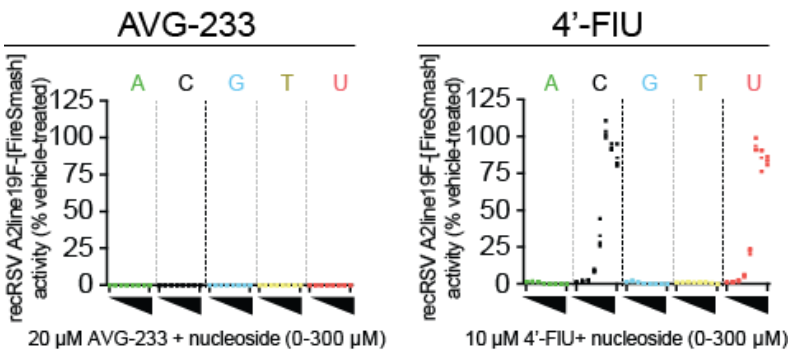

Fig. S7. Effect of endogenous nucleotides on AVG-233 RdRP inhibition. recRSV-fireSMASh-infected cells were treated with 20 µM of AVG-233 (left) or 10 µM of 4'-FlU (right) and serial dilutions of exogenous nucleosides were added to the extracellular media. Viral replication was determined by reporter activity and normalized for replication in the presence of vehicle (DMSO) volume equivalents instead of AVG-233 or 4'-FlU. Symbols represent independent repeats (N=3).

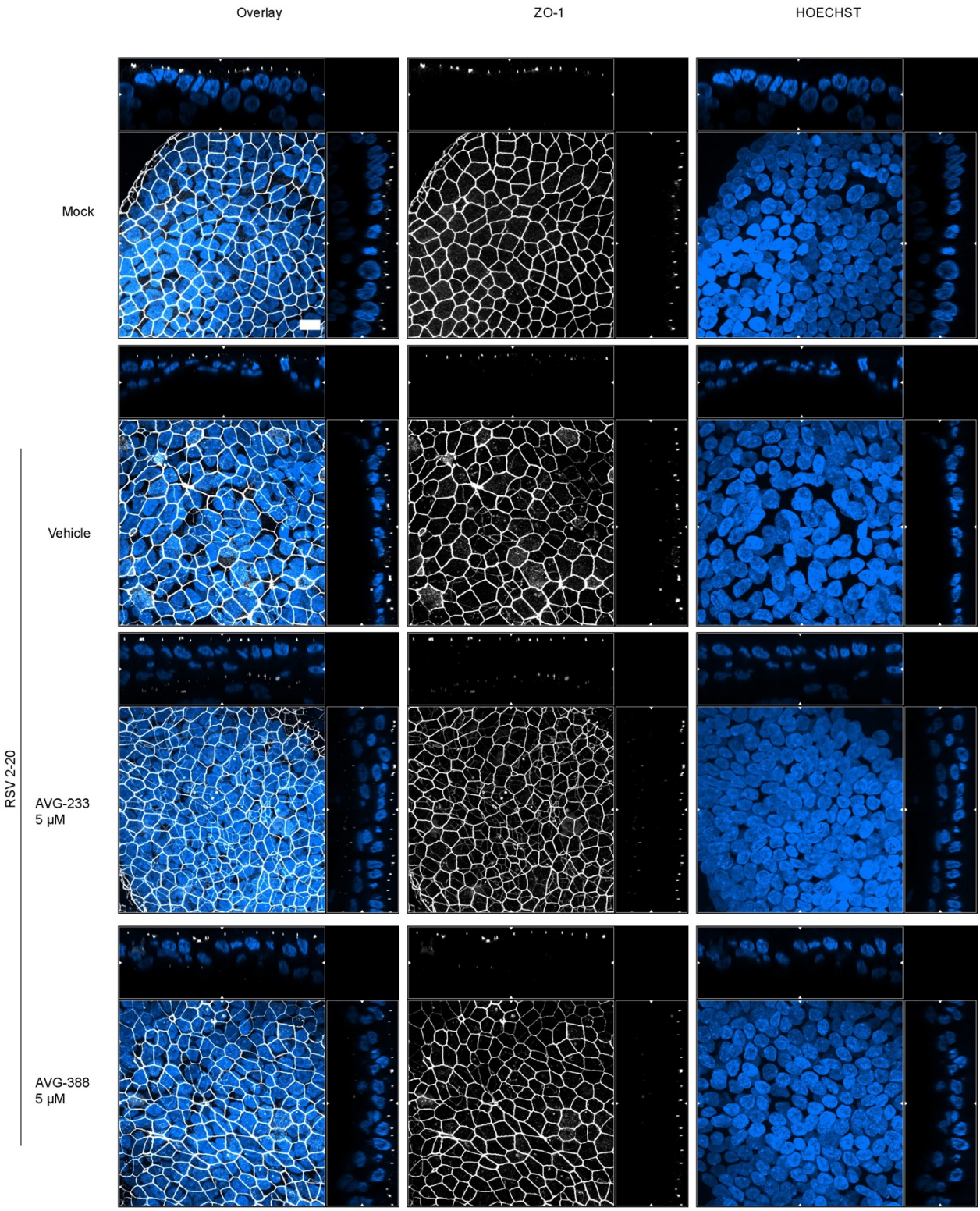

Fig. S8. Immunostaining of 3D-HAE. Tight junctions were detected with anti-ZO-I antibody (white). Cells were mock-infected or infected with recRSV-fireSMASh and treated with vehicle (0.1% DMSO) or AVG-233 or AVG-388 at 5 µM. Nuclei were stained with Hoechst 35443 (blue). Cultures were fixed and stained 3 days post-infection; scale bar 20 µm.

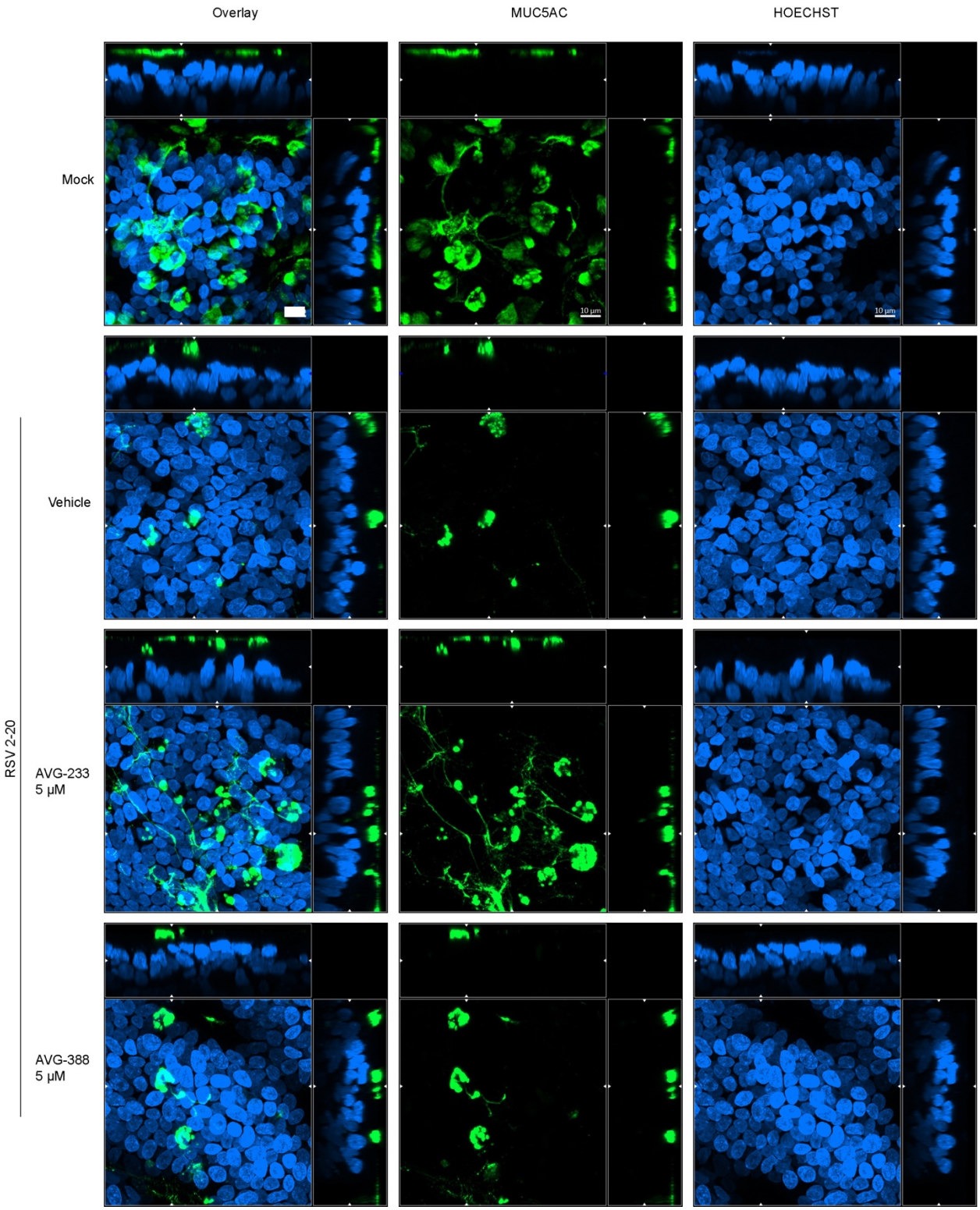

Fig. S9. Immunolabelling of 3D-HAE. Goblet cells were detected with anti-MUC5AC antibody (green). Cells were mock-infected or infected with recRSV-fireSMASh and treated with vehicle (0.1% DMSO) or AVG-233 or AVG-388 at 5 µM. Nuclei staining with Hoechst 35443 (blue). Cultures were fixed and stained 3 days post-infection; scale bar 20 µm.

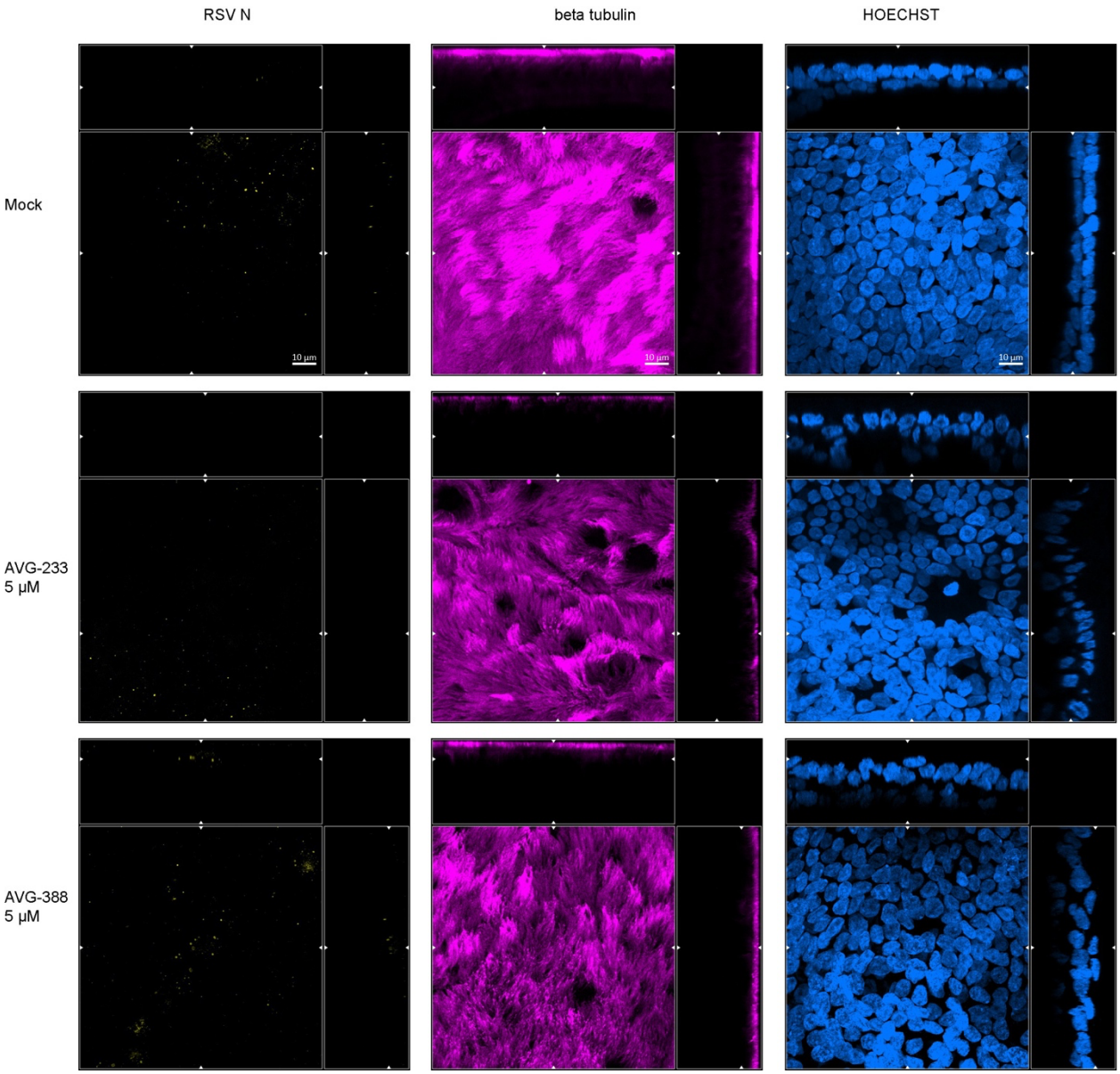

Fig. S10. Immunolabelling of 3D-HAE. Ciliated cells were detected with anti-beta-tubulin antibody (pink) and RSV-induced cytoplasmic inclusion bodies were detected with anti-RSV N (yellow). Cells were mock-infected or infected with recRSV-fireSMASh and treated with vehicle (0.1% DMSO) or AVG-233 or AVG-388 at 5 µM. Nuclei were stained with Hoechst 35443 (blue). Cultures were fixed and stained 3 days post-infection; scale bar 20 µm.

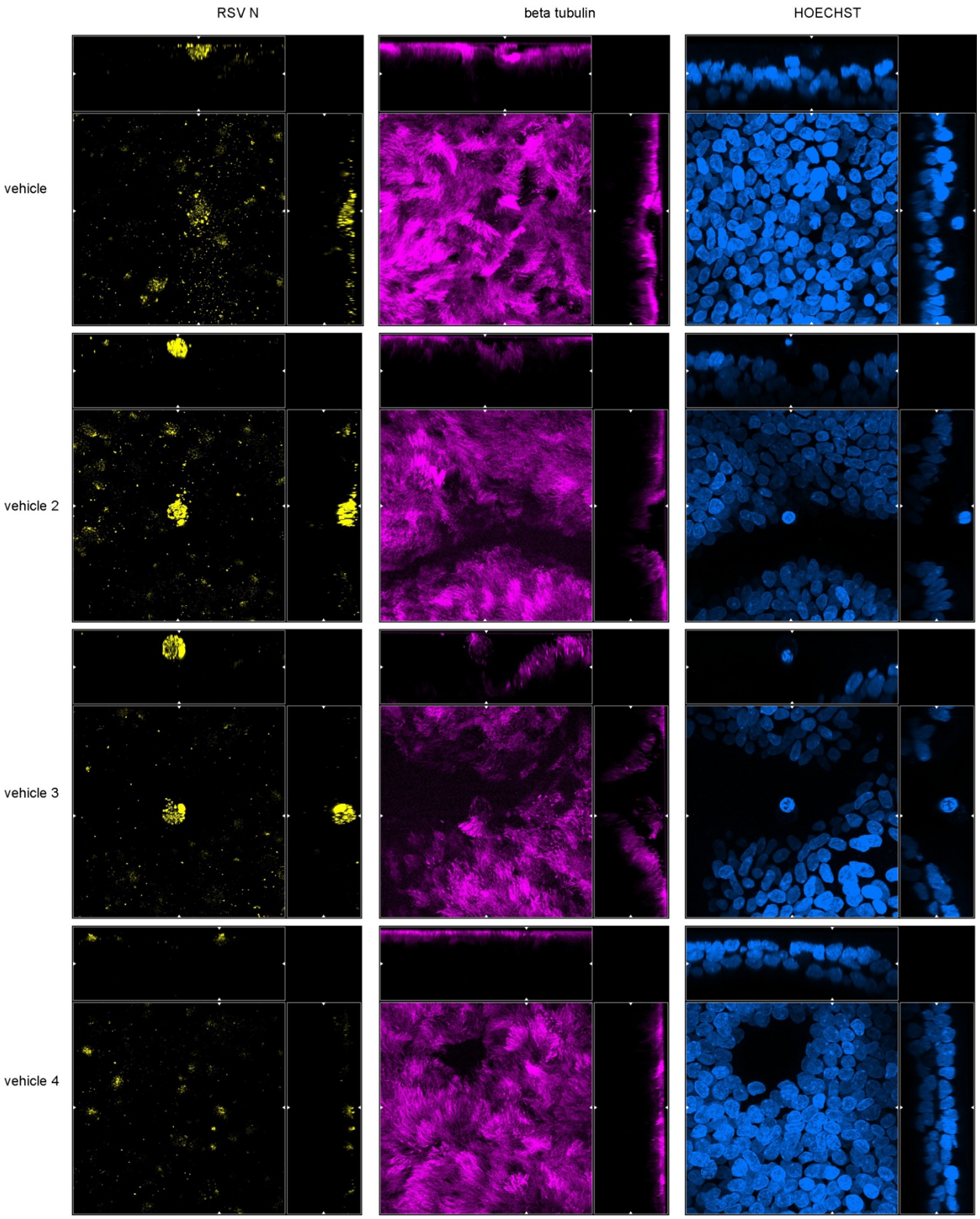

Fig. S11. Immunolabelling of 3D-HAE. Ciliated cells were detected with anti-beta-tubulin antibody (pink) and RSV-induced cytoplasmic inclusion bodies with anti-RSV N (yellow). Cells were mock-infected or infected with recRSV-fireSMASh and treated with vehicle (0.1% DMSO) or AVG-233 or AVG-388 at 5 µM. Nuclei were stained with Hoechst 35443 (blue). Cultures were fixed and stained 3 days post-infection; scale bar 20 µm.

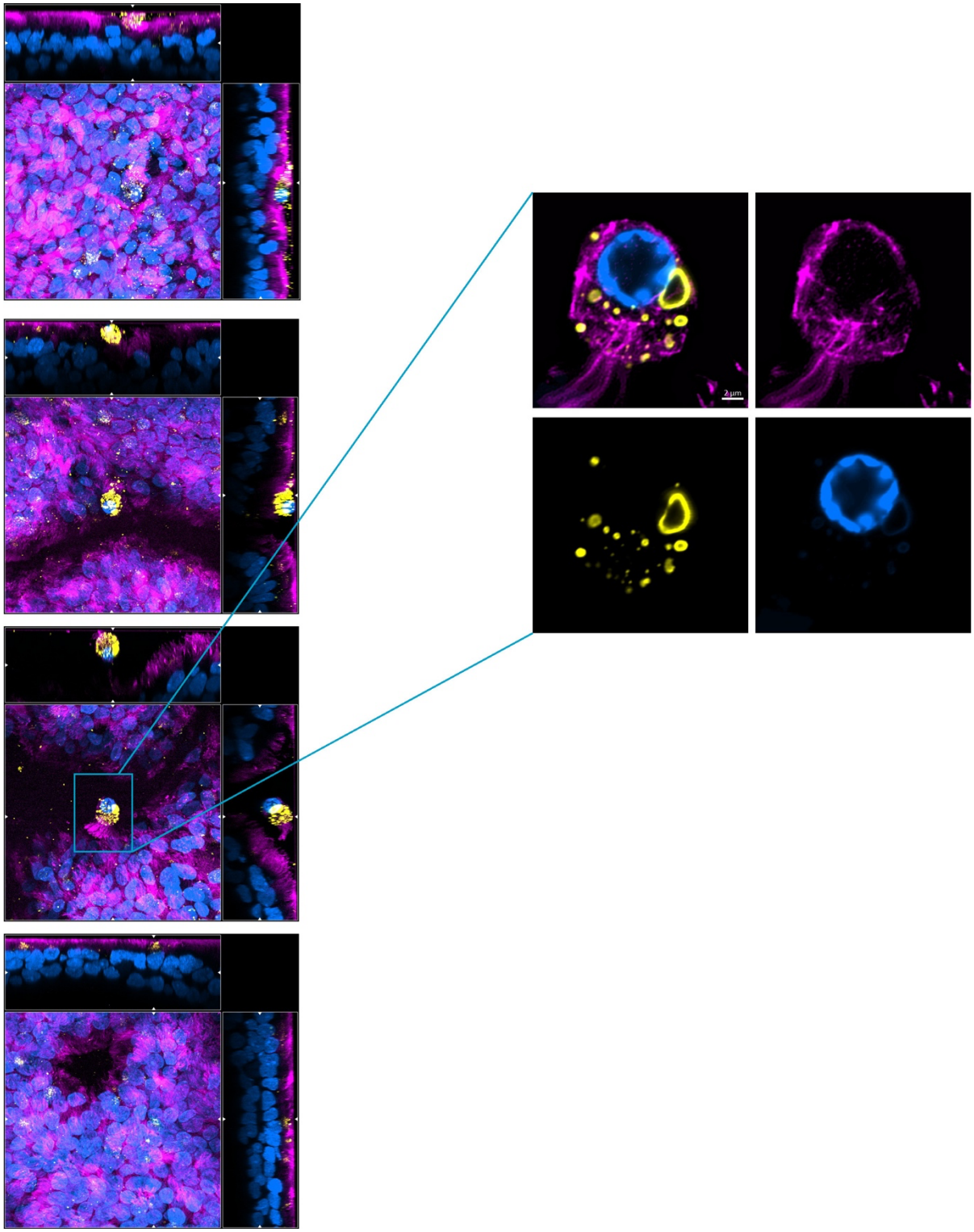

Fig. S12. Immunolabelling of 3D-HAE. Ciliated cells were detected with anti-beta-tubulin antibody (pink) and RSV-induced cytoplasmic inclusion bodies were detected with anti-RSV N (yellow). Cells were mock-infected or infected with recRSV-fireSMASh and treated with vehicle (0.1% DMSO) or AVG-233 or AVG-388 at 5 µM. Nuclei were stained with Hoechst 35443 (blue). Cultures were fixed and stained 3 days post-infection; scale bar 20 µm.

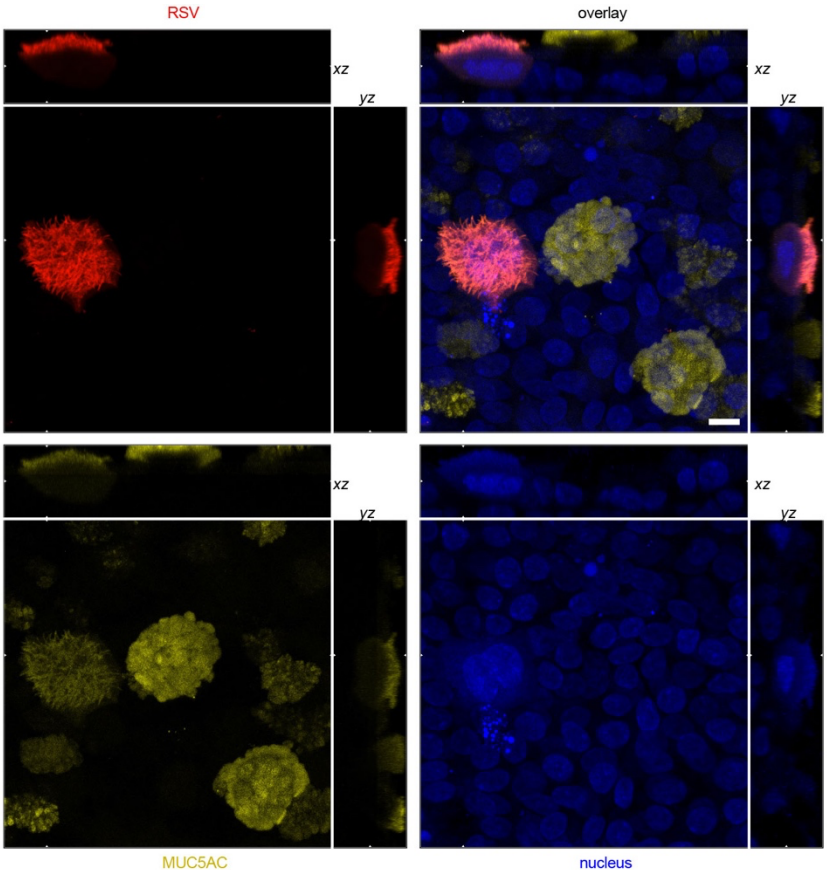

Fig. S13. Ciliated cells from 3D-HAE infected with recRSV-fireSMASh. RSV-infected cells were detected with a polyclonal anti-RSV antibody (red), mucus producing goblet cells were detected with specific anti-Muc5AC antibody (yellow), and nuclei were stained with DAPI (blue). Cultures were fixed and stained 10 days post-infection; scale bar 10 μm.

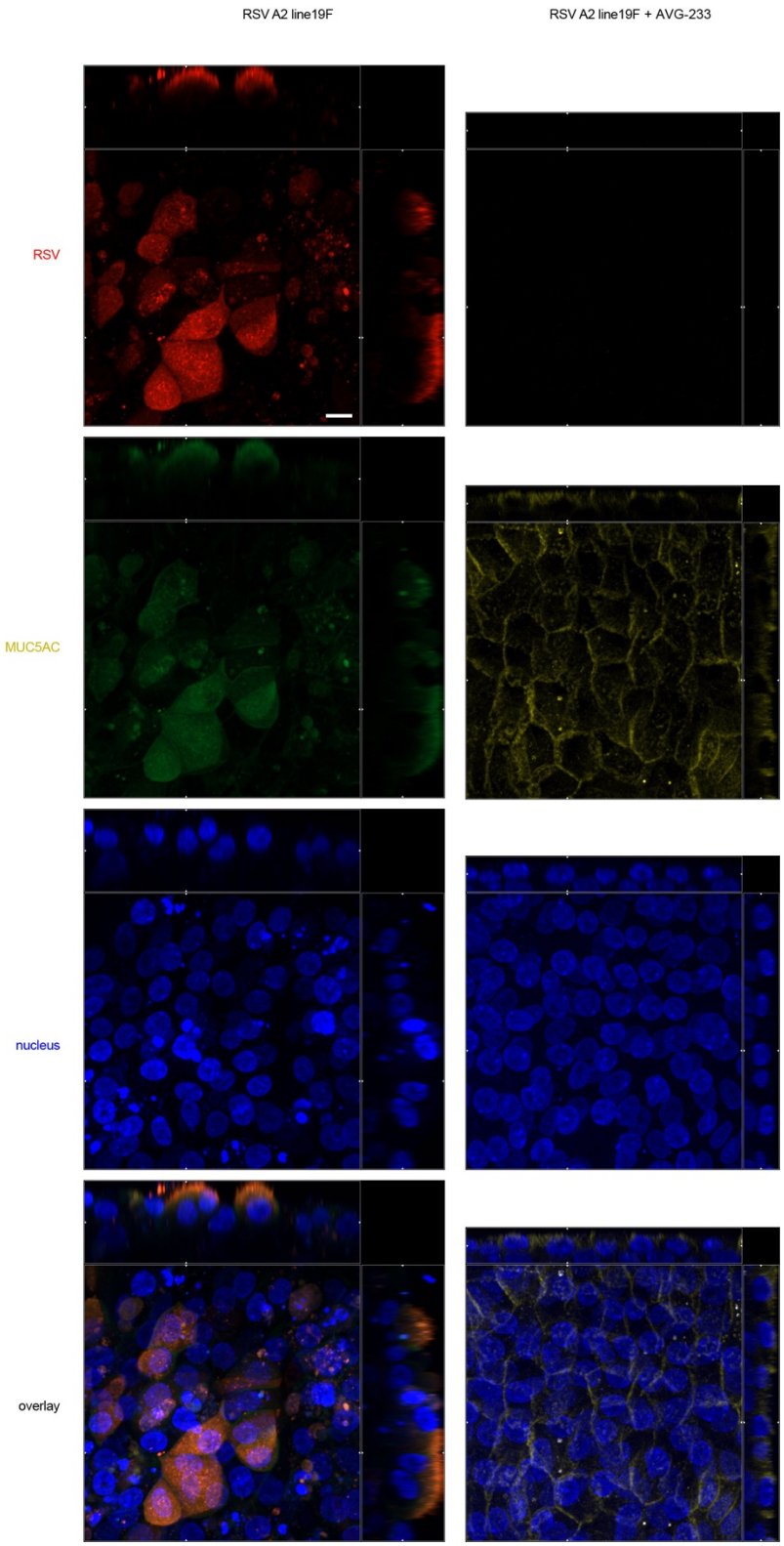

Fig. S14. Treatment with AVG-233 of 3D-HAEs infected with recRSV-fireSMASh. Adherens junction immunostaining is colored in yellow (anti-E-Cadherin), recRSV-fireSMASh infected cells immunostaining is colored in red (anti-RSV) and nucleus staining is colored in blue (DAPI); scale bar: 20 µm.

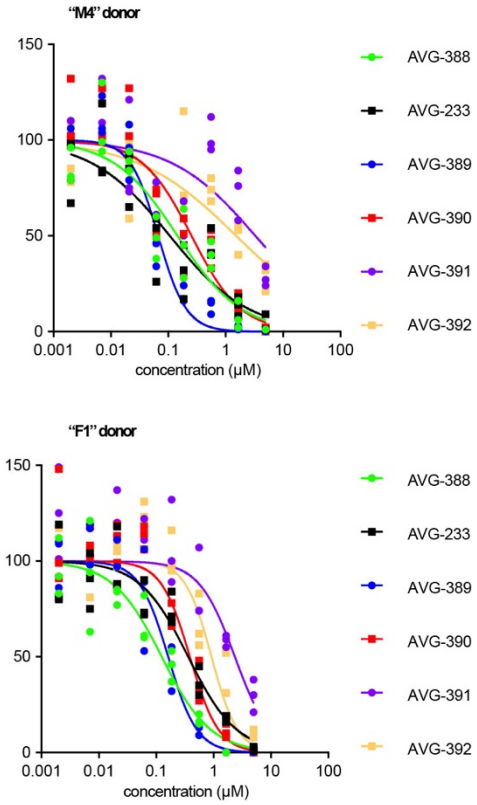

Fig. S15. Dose-response inhibition of recRSV-fireSMASh by analogs of AVG-233 in undifferentiated primary human airway epithelial cells. Top: "M4" donor, Bottom: "F1" donor. Values are normalized for vehicle-treated reactions; symbols represent individual biological repeats (n=3). EC_{50} values and 95% confidence intervals (shown in Table S1) are derived from 4-parameter variable slope regression models (solid line).

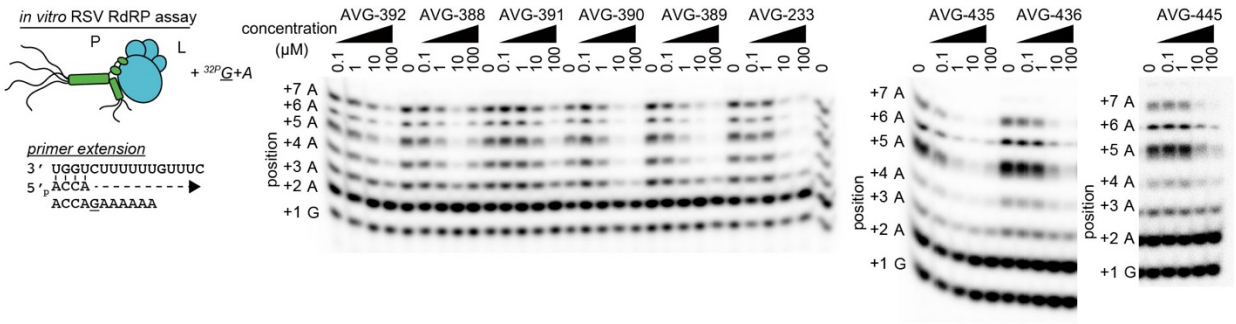

Fig. S16. Dose-response inhibition of *in vitro* RdRP primer extension by analogs of AVG-233. Representative autoradiograms (n=3).

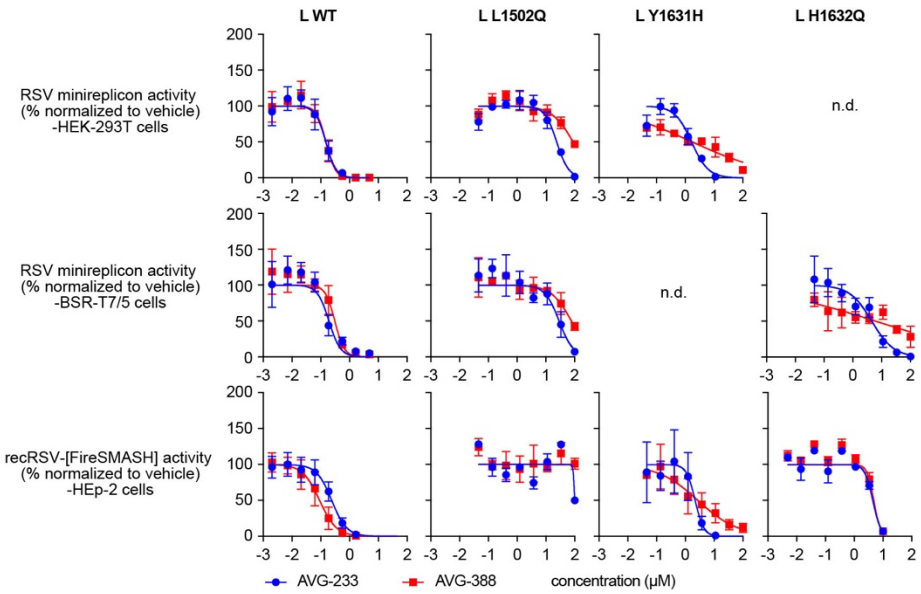

Fig. S17. Side-by-side comparison of AVG-233 and AVG-388 dose-response inhibition of either RSV minireplicon (top) and recRSV-fireSMASh (bottom). Minireplicon assays were performed either in HEK-293T cells or BSR-T7/5 cells. Values are normalized for vehicle-treated reactions; symbols represent individual biological repeats (n=3). EC_{50} values and 95% confidence intervals are derived from 4-parameter variable slope regression models (solid line).

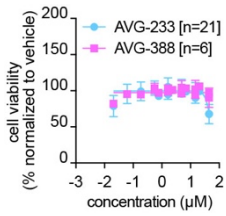

Fig. S18. Comparison of AVG-233 and AVG-388 cytotoxicity. Dose-response assays; Symbols represent means of individual biological repeats ± SD.

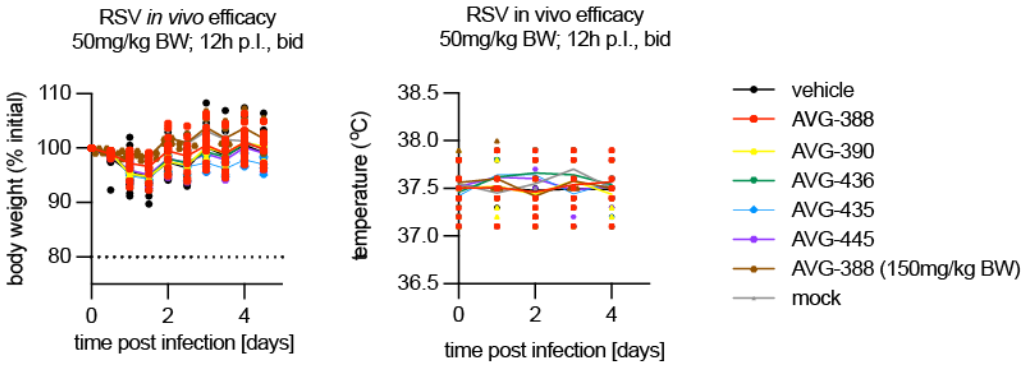

Fig. S19. Mouse bodyweight and temperature. Clinical signs of animals from the efficacy studies shown in Fig. 5 F-I. Animals were treated orally with 50 mg/kg b.i.d. or 150 mg/kg b.i.d. (AVG-388 high dose only), and body weight and temperature determined. Symbols represent individual biological repeats (individual animals), lines connect group means.

10x

AVG-388 treated

animal 1

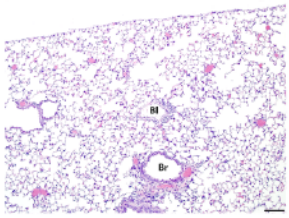

animal 2

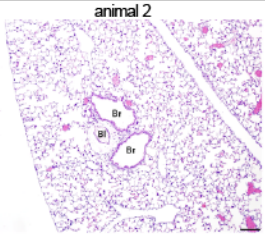

animal 3

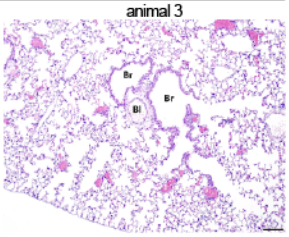

vehicle treated

animal 4

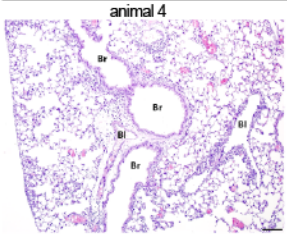

animal 5

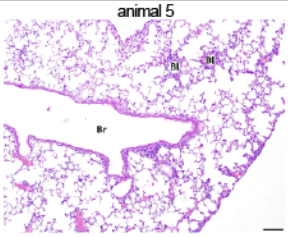

animal 6

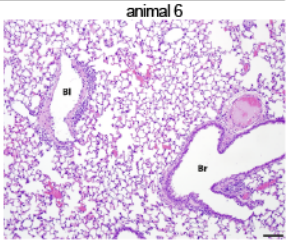

mock infected

animal 7

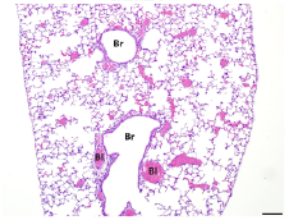

animal 8

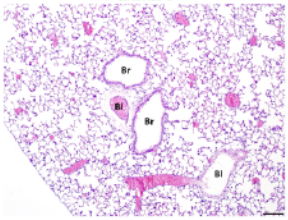

20x

AVG-388 treated

animal 1

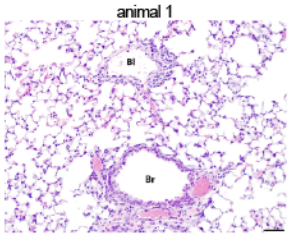

animal 2

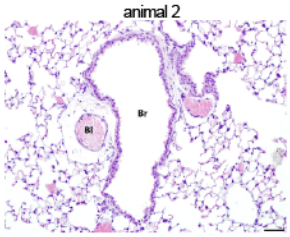

animal 3

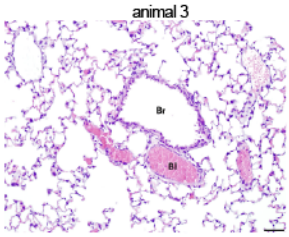

vehicle treated

animal 4

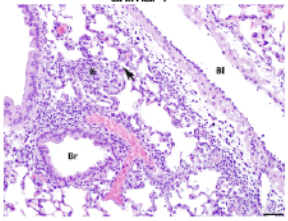

animal 5

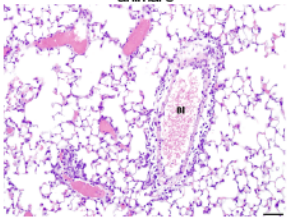

animal 6

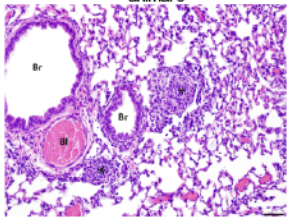

mock infected

animal 7

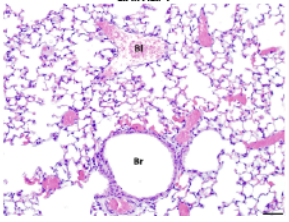

animal 8

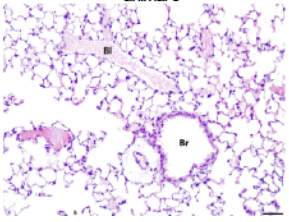

Fig. S20. Lung histopathology. Photomicrographs of lung sections extracted 4.5 days after infection of animals and subjected to H&E staining, shown at 10× (top; scale bar 100 μm) and 20× (bottom; scale bar 50 μm) magnification. n=3 per treatment group; mock-infected animals (mock; n=2) received buffered saline instead of virus inoculum. Bl, blood vessel; Br, bronchiole; arrow, interstitial pneumonia; asterisks, alveolitis.

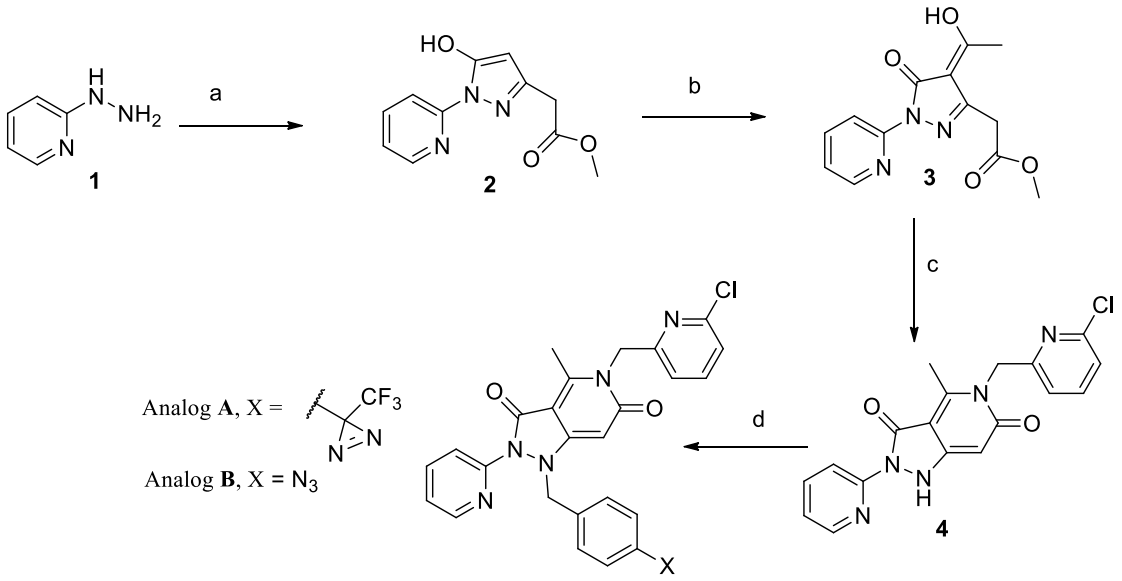

Fig. S21. Schematic of the chemical synthesis strategy of the AVG scaffold. Reagents and conditions to generate analogs **A** and **B** from compound **1** with intermediates **2**, **3**, and **4** were (a) Dimethyl 1,3-acetonedicarboxylate, toluene, reflux, 12 hours, 90%; (b) $MeC(OEt)_3$, AcOH, CH_3CN, 70°C, 12 hours; (c) (6-Chloropyridin-2-yl)methanamine dihydrochloride, DIPEA, CH_3CN, 2 hours, DBU, 2-4 hours, 35%; and (d) substituted benzyl halide, DIPEA, 50°C, 2-3 hours, 40-50%.

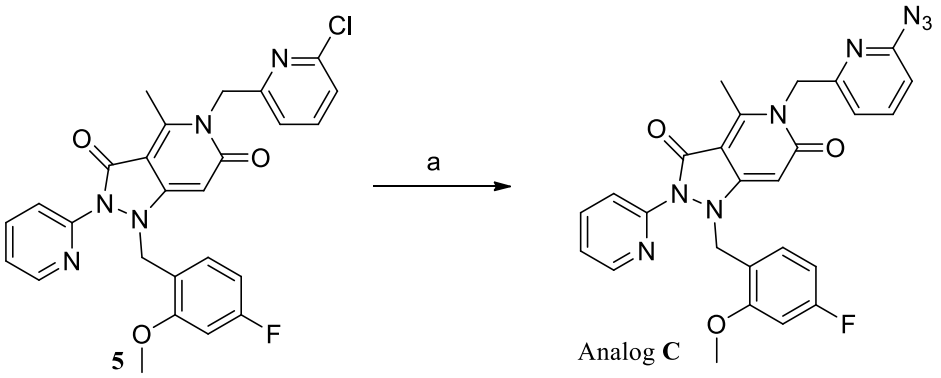

Fig. S22. Schematic of the chemical synthesis strategy of AVG analog C. Reagents and conditions to generate analog **C** from compound **5** (prepared as shown in Fig. S21) were (a) NaN_3, NH_4Cl, DMF, 48 hours, 110°C, 36%.

Table S1.

	Cell line or type												*in vitro* RdRP	
	HEp-2				"F1" HAE				"M4" HAE					
Compound	EC_{50} (μM)	95% CI	CC_{50} (μM)	95% CI	EC_{50} (μM)	95% CI	CC_{50} (μM)	95% CI	EC_{50} (μM)	95% CI	CC_{50} (μM)	95% CI	IC_{50} (μM)	95% CI
AVG-233	0.24	0.21 to 0.27	>50	>50	0.36	0.25 to 0.52	>45	>45	0.11	0.06 to 0.20	>45	>45	6.83	3.36 to 14.58
AVG-388	0.05	0.05 to 0.06	>10	>10	0.13	0.09 to 0.18	>10	>10	0.15	0.09 to 0.25	>10	>10	1.25	0.15 to 21568
AVG-389	0.09	0.09 to 0.10	>5	>5	0.16	0.12 to 0.2149	>45	>45	0.07	0.05 to 0.10	>45	>45	1.88	0.60 to 6.60
AVG-390	0.11	0.10 to 0.13	>45	>45	0.39	0.27 to 0.56	>45	>45	0.25	0.12 to 0.57	>45	>45	4.62	1.69 to 14.10
AVG-391	0.96	0.79 to 1.18	>45	>45	2.35	1.29 to 5.01	>45	>45	3.30	1.21 to 35.02	>45	>45	17.39	15.89 to 19.04
AVG-392	0.81	0.71 to 0.93	>45	>45	0.92	0.64 to 1.33	>45	>45	1.53	0.54 to 8.83	>45	>45	23.11	15.30 to 35.74
AVG-435	0.2	0.15 to 0.27	>5	>5	nd	nd	nd	nd	nd	nd	nd	nd	0.89	0.29 to 3.20
AVG-436	0.08	0.07 to 0.11	>5	>5	nd	nd	nd	nd	nd	nd	nd	nd	4.63	2.12 to 10.65
AVG-445	0.2	0.15 to 0.26	>5	>5	nd	nd	nd	nd	nd	nd	nd	nd	5.53	1.28 to 37.21

Efficacy of AVG series *in vitro*. Dose response inhibition assays of recRSV-fireSMASh incubated with selected AVG-233 fluorine and chlorine analogs in a human cell line or primary human airway epithelium cells (CI, confidence interval; nd, not determined).

Table S2.

Assay	Cell line	RSV L	AVG-233 EC_{50}	95% CI	AVG-388 EC_{50}	95% CI
minireplicon[a]	HEK-293T	WT	0.15	0.11 to 0.19	0.15	0.12 to 0.19
minireplicon[a]	HEK-293T	L1502Q	24.04	18.46 to 30.95	89.45	61.84 to 161.4
minireplicon[a]	BSR T7/5	WT	0.19	0.13 to 0.32	0.31	(-)
minireplicon[a]	BSR T7/5	L1502Q	29.16	18.03 to 45.81	78.2	52.38 to 147.3
minireplicon[a]	BSR T7/5	H1632Q	4.57	2.85 to 7.17	6.24	1.87 to 33.15
recombinant[b]	HEp-2	WT	0.24	0.23 to 0.25	0.09	0.08 to 0.10
recombinant[b]	HEp-2	L1502Q	>100.0	>100.0	>100.0	>100.0
recombinant[b]	HEp-2	Y1631H	2.19	(-)	2.72	1.43 to 5.26
recombinant[b]	HEp-2	H1632Q	4.42	(-)	4.81	(-)

Comparison of AVG-233 and AVG-388 resistance profiles. Minireplicon activity[a] and recRSV-fireSMASh[b] activity in the presence or absence of resistance mutations in RSV L (CI, confidence interval).

Table S3.

compound	dose	Lung viral load reduction (log10 $TCID_{50}$/ml) relative to vehicle-treated	SD
AVG-233	50 mg/kg bid	-0.44	0.38
AVG-388	50 mg/kg bid	-1.3	0.25
AVG-388	150 mg/kg bid	-1.9	0.23
AVG-389	nd	nd	nd
AVG-390	50 mg/kg bid	-0.5	0.26
AVG-391	nd	nd	nd
AVG-392	nd	nd	nd
AVG-435	50 mg/kg bid	-0.44	0.36
AVG-436	50 mg/kg bid	-0.89	0.14
AVG-445	50 mg/kg bid	-1.1	0.16

Efficacy of AVG series *in vivo*. Lung viral load 4.5 days post-infection after therapeutic treatment (10 hours after infection).

Data S1. Source data file containing all quantitative raw data for main and supplementary figures.

REFERENCES AND NOTES

1. T. Shi, D. A. McAllister, K. L. O'Brien, E. A. F. Simoes, S. A. Madhi, B. D. Gessner, F. P. Polack, E. Balsells, S. Acacio, C. Aguayo, I. Alassani, A. Ali, M. Antonio, S. Awasthi, J. O. Awori, E. Azziz-Baumgartner, H. C. Baggett, V. L. Baillie, A. Balmaseda, A. Barahona, S. Basnet, Q. Bassat, W. Basualdo, G. Bigogo, L. Bont, R. F. Breiman, W. A. Brooks, S. Broor, N. Bruce, D. Bruden, P. Buchy, S. Campbell, P. Carosone-Link, M. Chadha, J. Chipeta, M. Chou, W. Clara, C. Cohen, E. de Cuellar, D. A. Dang, B. Dash-Yandag, M. Deloria-Knoll, M. Dherani, T. Eap, B. E. Ebruke, M. Echavarria, C. C. de Freitas Lazaro Emediato, R. A. Fasce, D. R. Feikin, L. Feng, A. Gentile, A. Gordon, D. Goswami, S. Goyet, M. Groome, N. Halasa, S. Hirve, N. Homaira, S. R. C. Howie, J. Jara, I. Jroundi, C. B. Kartasasmita, N. Khuri-Bulos, K. L. Kotloff, A. Krishnan, R. Libster, O. Lopez, M. G. Lucero, F. Lucion, S. P. Lupisan, D. N. Marcone, J. P. McCracken, M. Mejia, J. C. Moisi, J. M. Montgomery, D. P. Moore, C. Moraleda, J. Moyes, P. Munywoki, K. Mutyara, M. P. Nicol, D. J. Nokes, P. Nymadawa, M. T. da Costa Oliveira, H. Oshitani, N. Pandey, G. Paranhos-Baccala, L. N. Phillips, V. S. Picot, M. Rahman, M. Rakoto-Andrianarivelo, Z. A. Rasmussen, B. A. Rath, A. Robinson, C. Romero, G. Russomando, V. Salimi, P. Sawatwong, N. Scheltema, B. Schweiger, J. A. G. Scott, P. Seidenberg, K. Shen, R. Singleton, V. Sotomayor, T. A. Strand, A. Sutanto, M. Sylla, M. D. Tapia, S. Thamthitiwat, E. D. Thomas, R. Tokarz, C. Turner, M. Venter, S. Waicharoen, J. Wang, W. Watthanaworawit, L. M. Yoshida, H. Yu, H. J. Zar, H. Campbell, H. Nair; RSV Global Epidemiology Network, Global, regional, and national disease burden estimates of acute lower respiratory infections due to respiratory syncytial virus in young children in 2015: A systematic review and modelling study. *Lancet* **390**, 946–958 (2017).

2. N. I. Mazur, D. Higgins, M. C. Nunes, J. A. Melero, A. C. Langedijk, N. Horsley, U. J. Buchholz, P. J. Openshaw, J. S. McLellan, J. A. Englund, A. Mejias, R. A. Karron, E. A. Simoes, I. Knezevic, O. Ramilo, P. A. Piedra, H. Y. Chu, A. R. Falsey, H. Nair, L. Kragten-Tabatabaie, A. Greenough, E. Baraldi, N. G. Papadopoulos, J. Vekemans, F. P. Polack, M. Powell, A. Satav, E. E. Walsh, R. T. Stein, B. S. Graham, L. J. Bont; Respiratory Syncytial Virus Network (ReSViNET) Foundation, The respiratory syncytial virus vaccine landscape:

Lessons from the graveyard and promising candidates. *Lancet Infect. Dis.* **18**, e295–e311 (2018).

3. J. Gottlieb, F. Torres, T. Haddad, G. Dhillon, D. Dilling, C. Knoop, R. Rampolla, R. Walia, V. Ahya, R. Kessler, A phase 2b randomized controlled trial of presatovir, an oral RSV fusion inhibitor, for the treatment of respiratory syncytial virus (RSV) in lung transplant (LT) recipients. *J. Heart Lung Transplant.* **37**, S155 (2018).

4. D. Hanfelt-Goade, N. Maimon, A. Nimer, F. Riviere, E. Catherinot, M. Ison, S. Jeong, E. Walsh, A. Gafter-Gvili, S. Nama, A phase 2b, randomized, double-blind, placebo-controlled trial of Presatovir (GS-5806), a novel Oral RSV fusion inhibitor, for the treatment of respiratory syncytial virus (RSV) in hospitalized adults, in *C17. New Insights in Acute Pulmonary Infections* (American Thoracic Society, 2018), p. A4457.

5. D. Yan, S. Lee, V. D. Thakkar, M. Luo, M. L. Moore, R. K. Plemper, Cross-resistance mechanism of respiratory syncytial virus against structurally diverse entry inhibitors. *Proc. Natl. Acad. Sci. U.S.A.* **111**, E3441–E3449 (2014).

6. Palivizumab, a humanized respiratory syncytial virus monoclonal antibody, reduces hospitalization from respiratory syncytial virus infection in high-risk infants. The IMpact-RSV Study Group. *Pediatrics* **102**, 531–537 (1998).

7. T. F. Feltes, A. K. Cabalka, H. C. Meissner, F. M. Piazza, D. A. Carlin, F. H. Top Jr., E. M. Connor, H. M. Sondheimer; Cardiac Synagis Study Group, Palivizumab prophylaxis reduces hospitalization due to respiratory syncytial virus in young children with hemodynamically significant congenital heart disease. *J. Pediatr.* **143**, 532–540 (2003).

8. M. Aggarwal, R. K. Plemper, Structural insight into paramyxovirus and pneumovirus entry inhibition. *Viruses* **12**, 342 (2020).

9. R. Fearns, R. K. Plemper, Polymerases of paramyxoviruses and pneumoviruses. *Virus Res.* **234**, 87–102 (2017).

10. H. Grosfeld, M. G. Hill, P. L. Collins, RNA replication by respiratory syncytial virus (RSV) is directed by the N, P, and L proteins; transcription also occurs under these conditions but requires RSV superinfection for efficient synthesis of full-length mRNA. *J. Virol.* **69**, 5677–5686 (1995).

11. J. Sourimant, M. A. Rameix-Welti, A. L. Gaillard, D. Chevret, M. Galloux, E. Gault, J. F. Eleouet, Fine mapping and characterization of the L-polymerase-binding domain of the respiratory syncytial virus phosphoprotein. *J. Virol.* **89**, 4421–4433 (2015).

12. M. Galloux, G. Gabiane, J. Sourimant, C. A. Richard, P. England, M. Moudjou, M. Aumont-Nicaise, J. Fix, M. A. Rameix-Welti, J. F. Eleouet, Identification and characterization of the binding site of the respiratory syncytial virus phosphoprotein to RNA-free nucleoprotein. *J. Virol.* **89**, 3484–3496 (2015).

13. R. Fearns, P. L. Collins, Role of the M2-1 transcription antitermination protein of respiratory syncytial virus in sequential transcription. *J. Virol.* **73**, 5852–5864 (1999).

14. E. Burke, N. M. Mahoney, S. C. Almo, S. Barik, Profilin is required for optimal actin-dependent transcription of respiratory syncytial virus genome RNA. *J. Virol.* **74**, 669–675 (2000).

15. A. P. Oliveira, F. M. Simabuco, R. E. Tamura, M. C. Guerrero, P. G. Ribeiro, T. A. Libermann, L. F. Zerbini, A. M. Ventura, Human respiratory syncytial virus N, P and M protein interactions in HEK-293T cells. *Virus Res.* **177**, 108–112 (2013).

16. C. A. Richard, V. Rincheval, S. Lassoued, J. Fix, C. Cardone, C. Esneau, S. Nekhai, M. Galloux, M. A. Rameix-Welti, C. Sizun, J. F. Eleouet, RSV hijacks cellular protein phosphatase 1 to regulate M2-1 phosphorylation and viral transcription. *PLOS Pathog.* **14**, e1006920 (2018).

17. D. Cao, Y. Gao, C. Roesler, S. Rice, P. D'Cunha, L. Zhuang, J. Slack, M. Domke, A. Antonova, S. Romanelli, S. Keating, G. Forero, P. Juneja, B. Liang, Cryo-EM structure of the respiratory syncytial virus RNA polymerase. *Nat. Commun.* **11**, 368 (2020).

18. M. S. A. Gilman, C. Liu, A. Fung, I. Behera, P. Jordan, P. Rigaux, N. Ysebaert, S. Tcherniuk, J. Sourimant, J. F. Eleouet, P. Sutto-Ortiz, E. Decroly, D. Roymans, Z. Jin, J. S. McLellan, Structure of the respiratory syncytial virus polymerase complex. *Cell* **179**, 193–204.e14 (2019).

19. J. Chapman, E. Abbott, D. G. Alber, R. C. Baxter, S. K. Bithell, E. A. Henderson, M. C. Carter, P. Chambers, A. Chubb, G. S. Cockerill, P. L. Collins, V. C. Dowdell, S. J. Keegan, R. D. Kelsey, M. J. Lockyer, C. Luongo, P. Najarro, R. J. Pickles, M. Simmonds, D. Taylor, S. Tyms, L. J. Wilson, K. L. Powell, RSV604, a novel inhibitor of respiratory syncytial virus replication. *Antimicrob. Agents Chemother.* **51**, 3346–3353 (2007).

20. B. Bailly, C. A. Richard, G. Sharma, L. Wang, L. Johansen, J. Cao, V. Pendharkar, D. C. Sharma, M. Galloux, Y. Wang, R. Cui, G. Zou, P. Guillon, M. von Itzstein, J. F. Eleouet, R. Altmeyer, Targeting human respiratory syncytial virus transcription anti-termination factor M2-1 to inhibit in vivo viral replication. *Sci. Rep.* **6**, 25806 (2016).

21. G. S. Cockerill, J. A. D. Good, N. Mathews, State of the art in respiratory syncytial virus drug discovery and development. *J. Med. Chem.* **62**, 3206–3227 (2019).

22. J. Sourimant, C. M. Lieber, M. Aggarwal, R. M. Cox, J. D. Wolf, J. J. Yoon, M. Toots, C. Ye, Z. Sticher, A. A. Kolykhalov, L. Martinez-Sobrido, G. R. Bluemling, M. G. Natchus, G. R. Painter, R. K. Plemper, 4'-Fluorouridine is an oral antiviral that blocks respiratory syncytial virus and SARS-CoV-2 replication. *Science*, **375**, 161–167 (2022).

23. C. L. Tiong-Yip, L. Aschenbrenner, K. D. Johnson, R. E. McLaughlin, J. Fan, S. Challa, H. Xiong, Q. Yu, Characterization of a respiratory syncytial virus L protein inhibitor. *Antimicrob. Agents Chemother.* **58**, 3867–3873 (2014).

24. R. M. Cox, M. Toots, J. J. Yoon, J. Sourimant, B. Ludeke, R. Fearns, E. Bourque, J. Patti, E. Lee, J. Vernachio, R. K. Plemper, Development of an allosteric inhibitor class blocking RNA elongation by the respiratory syncytial virus polymerase complex. *J. Biol. Chem.* **293**, 16761–16777 (2018).

25. K. Sudo, Y. Miyazaki, N. Kojima, M. Kobayashi, H. Suzuki, M. Shintani, Y. Shimizu, YM-53403, a unique anti-respiratory syncytial virus agent with a novel mechanism of action. *Antiviral Res.* **65**, 125–131 (2005).

26. M. Coates, D. Brookes, Y. I. Kim, H. Allen, E. A. F. Fordyce, E. A. Meals, T. Colley, C. L. Ciana, G. F. Parra, V. Sherbukhin, J. A. Stockwell, J. C. Thomas, S. F. Hunt, L. Anderson-Dring, S. T. Onions, L. Cass, P. J. Murray, K. Ito, P. Strong, J. P. DeVincenzo, G. Rapeport, Preclinical characterization of PC786, an inhaled small-molecule respiratory syncytial virus L protein polymerase inhibitor. *Antimicrob. Agents Chemother.* **61**, e00737-17 (2017).

27. V. A. Laganas, E. F. Dunn, R. E. McLaughlin, C. L. Tiong-Yip, O. Yuzhakov, V. M. Isabella, P. Hill, Q. Yu, Characterization of novel respiratory syncytial virus inhibitors identified by high throughput screen. *Antiviral Res.* **115**, 71–74 (2015).

28. M. Dochow, S. A. Krumm, J. E. Crowe Jr., M. L. Moore, R. K. Plemper, Independent structural domains in paramyxovirus polymerase protein. *J. Biol. Chem.* **287**, 6878–6891 (2012).

29. O. Poch, I. Sauvaget, M. Delarue, N. Tordo, Identification of four conserved motifs among the RNA-dependent polymerase encoding elements. *EMBO J.* **8**, 3867–3874 (1989).

30. J. Fix, M. Galloux, M. L. Blondot, J. F. Eleouet, The insertion of fluorescent proteins in a variable region of respiratory syncytial virus L polymerase results in fluorescent and functional enzymes but with reduced activities. *Open Virol. J.* **5**, 103–108 (2011).

31. J. A. Horwitz, S. Jenni, S. C. Harrison, S. P. J. Whelan, Structure of a rabies virus polymerase complex from electron cryo-microscopy. *Proc. Natl. Acad. Sci. U.S.A.* **117**, 2099–2107 (2020).

32. S. Jenni, L. M. Bloyet, R. Diaz-Avalos, B. Liang, S. P. J. Whelan, N. Grigorieff, S. C. Harrison, Structure of the vesicular stomatitis virus L protein in complex with its phosphoprotein cofactor. *Cell Rep.* **30**, 53–60.e5 (2020).

33. B. Liang, Z. Li, S. Jenni, A. A. Rahmeh, B. M. Morin, T. Grant, N. Grigorieff, S. C. Harrison, S. P. J. Whelan, Structure of the L protein of vesicular stomatitis virus from electron cryomicroscopy. *Cell* **162**, 314–327 (2015).

34. R. J. Pickles, Human airway epithelial cell cultures for modeling respiratory syncytial virus infection. *Curr. Top. Microbiol. Immunol.* **372**, 371–387 (2013).

35. M. Toots, J.-J. Yoon, R. M. Cox, M. Hart, Z. M. Sticher, N. Makhsous, R. Plesker, A. H. Barrena, P. G. Reddy, D. G. Mitchell, R. C. Shean, G. R. Bluemling, A. A. Kolykhalov, A. L. Greninger, M. G. Natchus, G. R. Painter, R. K. Plemper, Characterization of orally efficacious influenza drug with high resistance barrier in ferrets and human airway epithelia. *Sci. Transl. Med.* **11**, eaax5866 (2019).

36. L. Zhang, M. E. Peeples, R. C. Boucher, P. L. Collins, R. J. Pickles, Respiratory syncytial virus infection of human airway epithelial cells is polarized, specific to ciliated cells, and without obvious cytopathology. *J. Virol.* **76**, 5654–5666 (2002).

37. V. Rincheval, M. Lelek, E. Gault, C. Bouillier, D. Sitterlin, S. Blouquit-Laye, M. Galloux, C. Zimmer, J. F. Eleouet, M. A. Rameix-Welti, Functional organization of cytoplasmic inclusion bodies in cells infected by respiratory syncytial virus. *Nat. Commun.* **8**, 563 (2017).

38. J. J. Yoon, M. Toots, S. Lee, M. E. Lee, B. Ludeke, J. M. Luczo, K. Ganti, R. M. Cox, Z. M. Sticher, V. Edpuganti, D. G. Mitchell, M. A. Lockwood, A. A. Kolykhalov, A. L. Greninger, M. L. Moore, G. R. Painter, A. C. Lowen, S. M. Tompkins, R. Fearns, M. G. Natchus, R. K. Plemper, Orally efficacious broad-spectrum ribonucleoside analog inhibitor of influenza and respiratory syncytial viruses. *Antimicrob. Agents Chemother.* **62**, e00766-18 (2018).

39. U.S. Food and Drug Administration, DA News Release Coronavirus (COVID-19) Update: FDA Authorizes Additional Oral Antiviral for Treatment of COVID-19 in Certain Adults (2021); https://www.fda.gov/news-events/press-announcements/coronavirus-covid-19-update-fda-authorizes-additional-oral-antiviral-treatment-covid-19-certain.

40. D. B. Madhura, J. Liu, B. Meibohm, R. E. Lee, Phase II metabolic pathways of spectinamide antitubercular agents: A comparative study of the reactivity of 4-substituted pyridines to glutathione conjugation. *Medchemcomm* **7**, 114–117 (2016).

41. J. Litchfield, R. Sharma, K. Atkinson, K. J. Filipski, S. W. Wright, J. A. Pfefferkorn, B. Tan, R. E. Kosa, B. Stevens, M. Tu, A. S. Kalgutkar, Intrinsic electrophilicity of the 4-methylsulfonyl-2-pyridone scaffold in glucokinase activators: Role of glutathione-S-transferases and in vivo quantitation of a glutathione conjugate in rats. *Bioorg. Med. Chem. Lett.* **20**, 6262–6267 (2010).

42. K. Inoue, T. Ohe, K. Mori, T. Sagara, Y. Ishii, M. Chiba, Aromatic substitution reaction of 2-chloropyridines catalyzed by microsomal glutathione S-transferase 1. *Drug Metab. Dispos.* **37**, 1797–1800 (2009).

43. J. R. Duvall, L. VerPlank, B. Ludeke, S. M. McLeod, M. D. Lee IV, K. Vishwanathan, C. A. Mulrooney, S. Le Quement, Q. Yu, M. A. Palmer, P. Fleming, R. Fearns, M. A. Foley, C. A. Scherer, Novel diversity-oriented synthesis-derived respiratory syncytial virus inhibitors identified via a high throughput replicon-based screen. *Antiviral Res.* **131**, 19–25 (2016).

44. S. L. Noton, K. Nagendra, E. F. Dunn, M. E. Mawhorter, Q. Yu, R. Fearns, Respiratory syncytial virus inhibitor AZ-27 differentially inhibits different polymerase activities at the promoter. *J. Virol.* **89**, 7786–7798 (2015).

45. R. M. Cox, J. Sourimant, M. Govindarajan, M. G. Natchus, R. K. Plemper, Therapeutic targeting of measles virus polymerase with ERDRP-0519 suppresses all RNA synthesis activity. *PLOS Pathog.* **17**, e1009371 (2021).

46. P. C. Jordan, C. Liu, P. Raynaud, M. K. Lo, C. F. Spiropoulou, J. A. Symons, L. Beigelman, J. Deval, Initiation, extension, and termination of RNA synthesis by a paramyxovirus polymerase. *PLOS Pathog.* **14**, e1006889 (2018).

47. J. Pan, X. Qian, S. Lattmann, A. El Sahili, T. H. Yeo, H. Jia, T. Cressey, B. Ludeke, S. Noton, M. Kalocsay, R. Fearns, J. Lescar, Structure of the human metapneumovirus polymerase phosphoprotein complex. *Nature* **577**, 275–279 (2020).

48. R. Abdella, M. Aggarwal, T. Okura, R. A. Lamb, Y. He, Structure of a paramyxovirus polymerase complex reveals a unique methyltransferase-CTD conformation. *Proc. Natl. Acad. Sci. U.S.A.* **117**, 4931–4941 (2020).

49. M. Ogino, N. Gupta, T. J. Green, T. Ogino, A dual-functional priming-capping loop of rhabdoviral RNA polymerases directs terminal de novo initiation and capping intermediate formation. *Nucleic Acids Res.* **47**, 299–309 (2019).

50. M. R. Braun, L. R. Deflube, S. L. Noton, M. E. Mawhorter, C. Z. Tremaglio, R. Fearns, RNA elongation by respiratory syncytial virus polymerase is calibrated by conserved region V. *PLOS Pathog.* **13**, e1006803 (2017).

51. A. L. Hotard, F. Y. Shaikh, S. Lee, D. Yan, M. N. Teng, R. K. Plemper, J. E. Crowe Jr., M. L. Moore, A stabilized respiratory syncytial virus reverse genetics system amenable to recombination-mediated mutagenesis. *Virology* **434**, 129–136 (2012).

52. D. Yan, M. Weisshaar, K. Lamb, H. K. Chung, M. Z. Lin, R. K. Plemper, Replication-competent influenza virus and respiratory syncytial virus luciferase reporter strains engineered for co-infections identify antiviral compounds in combination screens. *Biochemistry* **54**, 5589–5604 (2015).

53. B. Ludeke, R. Fearns, The respiratory syncytial virus polymerase can perform RNA synthesis with modified primers and nucleotide analogs. *Virology* **540**, 66–74 (2020).

54. S. L. Noton, L. R. Deflube, C. Z. Tremaglio, R. Fearns, The respiratory syncytial virus polymerase has multiple RNA synthesis activities at the promoter. *PLOS Pathog.* **8**, e1002980 (2012).

55. J. Schindelin, I. Arganda-Carreras, E. Frise, V. Kaynig, M. Longair, T. Pietzsch, S. Preibisch, C. Rueden, S. Saalfeld, B. Schmid, J. Y. Tinevez, D. J. White, V. Hartenstein, K. Eliceiri, P.

Tomancak, A. Cardona, Fiji: An open-source platform for biological-image analysis. *Nat. Methods* **9**, 676–682 (2012).

56. J. Deval, J. Hong, G. Wang, J. Taylor, L. K. Smith, A. Fung, S. K. Stevens, H. Liu, Z. Jin, N. Dyatkina, M. Prhavc, A. D. Stoycheva, V. Serebryany, J. Liu, D. B. Smith, Y. Tam, Q. Zhang, M. L. Moore, R. Fearns, S. M. Chanda, L. M. Blatt, J. A. Symons, L. Beigelman, Molecular basis for the selective inhibition of respiratory syncytial virus RNA polymerase by 2'-Fluoro-4'-chloromethyl-cytidine triphosphate. *PLOS Pathog.* **11**, e1004995 (2015).

57. E. P. Tchesnokov, P. Raeisimakiani, M. Ngure, D. Marchant, M. Gotte, Recombinant RNA-dependent RNA polymerase complex of ebola virus. *Sci. Rep.* **8**, 3970 (2018).

58. H. Chi, C. Liu, H. Yang, W. F. Zeng, L. Wu, W. J. Zhou, R. M. Wang, X. N. Niu, Y. H. Ding, Y. Zhang, Z. W. Wang, Z. L. Chen, R. X. Sun, T. Liu, G. M. Tan, M. Q. Dong, P. Xu, P. H. Zhang, S. M. He, Comprehensive identification of peptides in tandem mass spectra using an efficient open search engine. *Nat. Biotechnol.* **36**, 1059–1061 (2018).

59. S. A. Jablonski, C. D. Morrow, Mutation of the aspartic acid residues of the GDD sequence motif of poliovirus RNA-dependent RNA polymerase results in enzymes with altered metal ion requirements for activity. *J. Virol.* **69**, 1532–1539 (1995).